3D Deformation Capture via a Configurable Self-Sensing IMU Sensor Network

ZIHONG ZHOU and PEI CHEN, Zhejiang University - China Southern Power Grid Joint Research Centre on AI, Zhejiang University, China
YINYU LU, Zhejiang University, China
QIANG CUI, Tsinghua University, China
DEYING PAN, YILUN LIU, and JIAJI LI, Zhejiang University, China
YANG ZHANG, University of California, United States
YE TAO and XUANHUI LIU, Hangzhou City University, China
LINGYUN SUN, Zhejiang-Singapore Innovation and AI Joint Research Lab and Future Design Laboratory of Zhejiang University, China
GUANYUN WANG*, Zhejiang University, China

Motion capture technologies reconstruct human movements and have wide-ranging applications. Mainstream research on motion capture can be divided into vision-based methods and inertial measurement unit (IMU)-based methods. The vision-based methods capture complex 3D geometrical deformations with high accuracy, but they rely on expensive optical equipment and suffer from the line-of-sight occlusion problem. IMU-based methods are lightweight but hard to capture fine-grained 3D deformations. In this work, we present a configurable self-sensing IMU sensor network to bridge the gap between the vision-based and IMU-based methods. To achieve this, we propose a novel kinematic chain model based on the four-bar linkage to describe the minimum deformation process of 3D deformations. We also introduce three geometric priors, obtained from the initial shape, material properties and motion features, to assist the kinematic chain model in reconstructing deformations and overcome the data sparsity problem. Additionally, to further enhance the accuracy of deformation capture, we propose a fabrication method to customize 3D sensor networks for different objects. We introduce origami-inspired thinking to achieve the customization process, which constructs 3D sensor networks through a 3D–2D–3D digital–physical transition. The experimental results demonstrate that our method achieves comparable performance with state-of-the-art methods.

CCS Concepts: • **Human-centered computing** → **Interaction devices**; *Ubiquitous and mobile computing*; • **Hardware** → **Sensors and actuators**; *Sensor applications and deployments.*

*Corresponding Author: Guanyun Wang, guanyun@zju.edu.cn.

Authors' addresses: Zihong Zhou, zihongzhou@zju.edu.cn; Pei Chen, chenpei@zju.edu.cn, Zhejiang University - China Southern Power Grid Joint Research Centre on AI, Zhejiang University, China; Yinyu Lu, Zhejiang University, China, buliugu6@outlook.com; Qiang Cui, Tsinghua University, China, cui-q18@mails.tsinghua.edu.cn; Deying Pan, deyingp2@zju.edu.cn; Yilun Liu, yilun.liu@zju.edu.cn; Jiaji Li, lijiaji@zju.edu.cn, Zhejiang University, China; Yang Zhang, University of California, United States, yangzhang@ucla.edu; Ye Tao, taoye@zucc.edu.cn; Xuanhui Liu, liuxuanhui@zju.edu.cn, Hangzhou City University, China; Lingyun Sun, Zhejiang-Singapore Innovation and AI Joint Research Lab and Future Design Laboratory of Zhejiang University, China, sunly@zju.edu.cn; Guanyun Wang, Zhejiang University, China, guanyun@zju.edu.cn.

2474-9567/2023/3-ART42 $15.00
https://doi.org/10.1145/3580874

Additional Key Words and Phrases: deformation capture, motion capture, sensor network, self-sensing input device, inertial measurement unit, customization, origami-inspired design

ACM Reference Format:
Zihong Zhou, Pei Chen, Yinyu Lu, Qiang Cui, Deying Pan, Yilun Liu, Jiaji Li, Yang Zhang, Ye Tao, Xuanhui Liu, Lingyun Sun, and Guanyun Wang. 2023. 3D Deformation Capture via a Configurable Self-Sensing IMU Sensor Network. *Proc. ACM Interact. Mob. Wearable Ubiquitous Technol.* 7, 1, Article 42 (March 2023), 24 pages. https://doi.org/10.1145/3580874

1 INTRODUCTION

Motion capture systems record and analyze human movements. Motion capture technologies have been widely used in various applications such as virtual reality [15, 25, 38], health monitoring [7, 17, 28], gait analyzing [56, 95], sports monitoring [77, 89], and film animation [47, 80]. Mainstream motion capture technologies can be divided into vision-based and IMU-based methods.

Vision-based methods (e.g., multi-camera systems [103] and marker-based solutions [20]) are capable of capturing complex 3D geometric deformations with high accuracy. The advantage of vision-based methods in deformation capture tasks comes from the rich information provided by cameras [9, 36, 97]. Essentially, a camera is the large-scale integration of ultrahigh-resolution pixel image sensor arrays. Vision-based methods can utilize enough image information and depth information in reconstructing 3D deformations. However, they rely on expensive auxiliary equipment, which suffers from large sizes and line-of-sight occlusions [49, 52]. Thus, vision-based motion capture systems are usually limited to lab or studio scenarios.

Comparatively, IMU-based motion capture systems are lightweight and low-cost, and have no limitations on line-of-sight shielding [71]. These advantages enable them to be more consumer-friendly and applicable for human-computer interaction applications [6, 49, 56]. Nevertheless, current non-optical sensing technologies, including IMU-based methods, are hard to integrate large-scale sensor nodes or sensor arrays to obtain dense information. IMU-based motion capture methods are effective at reconstructing human limb movements based on the motion information captured by sparse sensor nodes [49]. These methods usually deploy a sensor node on each limb and only use the sensor to measure the angle of the limb, regardless of its exact location. Such deployment methods are unsuitable for fine-grained deformation capture because imprecise positions of sensor nodes will introduce random measurement errors, which reduces the accuracy of deformation capture. Thus, current IMU-based motion capture systems mainly focus on detecting human limb movements [43] and are hard to capture fine-grained deformations for a wider range of applications. Here, the fine-grained deformations denote complex geometric deformations such as 3D curve deformations or 3D surface deformations, not only the segmented deformations like body segment movements.

Therefore, it is necessary to bridge the gap between the vision-based and IMU-based methods to offer a lightweight and high-accuracy deformation capture solution. To achieve this, we aim to address the data sparsity problem and the sensor nodes' deployment problem in an IMU sensor network.

In this work, we propose a self-sensing algorithm that can accurately and robustly reconstruct both global motions and fine-grained 3D deformations using sparse motion data obtained from an IMU sensor network. All sensor nodes of the sensor network are placed on the surface of the measured object in a sparse distribution. Deformations occurring between two adjacent sensor nodes are regarded as a measurable minimum deformation unit. We propose a novel kinematic chain model based on the four-bar linkage to describe this minimum deformation process. This model calculates relative spatial positions between adjacent sensor nodes based on three geometric priors. Specifically, the shape-associated geometric prior contains the initial positions and orientations of sensor nodes placed on the surface of the object to be measured. The other two priors are based on the material properties and motion features of a 3D sensor network respectively. The proposed algorithm supports a reliable, accurate, and real-time self-sensing of the sensor network.

In addition, we introduce origami-inspired thinking [35] to achieve the customization of 3D sensor networks. The customized sensor networks can accommodate varying shape measurements by providing precise position constraints for sensor nodes, thereby reducing deformation measurement errors. The construction process of sensor networks can be regarded as a 3D–2D–3D digital–physical transition process. Specifically, in the process of 3D-2D, we acquire the 3D mesh model of the object to be measured and unfold it into a 2D planar mesh model while maintaining all geometric information. In the digital-physical transition process, we fabricate the planar meshes using laser-cutting technology. Finally, in the 2D-3D transform process, we assemble the planar meshes with sensor nodes to construct a 3D sensor network. Such a customized 3D sensor network not only fits the shape of the measured object, but also provides effective geometric constraints for real-time capture.

To evaluate our method, we conduct three experiments on different deformation capture tasks, including the 3D curve deformation capture, the 3D surface deformation capture, and the arm motion and deformation capture, respectively. The experimental results demonstrate that our method achieves comparable performance (average error at 4.59mm, average error rate at 1.40%) with state-of-the-art methods. Our method supports the development of various emerging interactive systems, such as wearable input devices, smart tangible user interfaces and complex shape measurement tools. Our contributions are summarized as below.

- We propose a self-sensing algorithm to reconstruct both global movements and fine-grained 3D deformations via an IMU sensor network. It uses a novel kinematic chain model based on the four-bar linkage to describe the minimum deformation process of 3D deformations.
- We introduce three geometric priors to corporate with the kinematic chain model to capture minor deformations, and to address the problem of data sparsity that occurred in the IMU sensor network.
- We design an efficient customized construction pipeline to build tailor-made 3D sensor networks for different shapes. It incorporates origami-inspired thinking and constructs 3D sensor networks through a 3D–2D–3D digital–physical transition process.

2 BACKGROUND AND RELATED WORK

2.1 Vision-based Methods for Deformation Capture

Vision-based methods for deformation capture are widely used in film and animation production to help understand human behaviors or produce high-quality 3D virtual characters [8]. Common vision-based methods contain marker-based systems [20], multi-camera systems [37, 102, 103], laser scanners [83] and radio-based systems [18]. These systems capture human motions with high accuracy and resolution. However, they rely on sophisticated hardware and strict system initialization [103], which are usually unaffordable and difficult for most unprofessional people.

Therefore, researchers pay more attention to using a monocular RGB or RGBD camera to capture and reconstruct high-quality 3D human motion [11, 40, 85]. For example, Choi et al. [11] presented a temporally consistent mesh recovery system (TCMR) to reconstruct temporally consistent 3D human poses from a video. Nevertheless, monocular cameras are still inevitably susceptible to visual clutter, occlusions and ambient light effects, which limits their applications in interactive scenarios [21]. Comparing with vision-based methods, the following self-sensing methods are more lightweight and portable, and support more flexible applications.

2.2 Self-sensing Methods for Deformation Capture

The self-sensing methods are mainstream non-visual approaches for deformation capture [10, 14, 21, 60, 64, 73, 79]. These methods usually construct self-sensing input devices using various contact-based sensors. Such devices have the capability of measuring their own deformation without external auxiliary equipment. We summarize existing deformation capture methods based on different sensing principles in Table 1.

Table 1. Existing works for deformation capture in different sensing principles.

Sensor Type	Spatial Dimensions of Sensor Data	Sensing Principle	Key Features
Resistance	1D, 2D	The sensors convert the shape or structure changes (stretching, bending, pressing, etc.) into the corresponding changes in the electric resistance values [75].	• Low-cost with the widest applications [5, 10, 19, 44, 48]. • Significant drifts over time [1, 34, 79].
Capacitance	1D, 2D	The geometrical changes of sensors affect the overlapping area of capacitance units, resulting in variations in capacitance values [79].	• Flexible and responsive [70, 96]. • Widely used in wearable electronics [22, 82, 100, 101, 104].
Piezoelectricity	1D, 2D	The deformations of a piezo element change the surface charge density of the material and produce weak polarized electrical signals with different applied stress [39, 72].	• Operate without power supplies [76, 78, 81]. • High sensitivity for dynamic deformations [12, 39].
Optical fiber	1D, 2D	When an optical fiber is under stress, its curvature radius and bending direction change, leading to changes in intensity, phase, wavelength or polarization of output light [64].	• Lightweight, compact and precise [3, 34, 64]. • Immunity to electromagnetic interference and applicable to harsh environments [16, 53, 92, 94]. • Require expensive equipment for sophisticated signal processing [2].
IMU	3D	IMU sensors detect 3D orientation information using accelerometers, gyroscopes, magnetometers or their combinations [32, 55].	• Suffer from data drift [24]. • Compact and lightweight [14].

Except for IMU-based methods, other self-sensing methods only capture 1D or 2D spatial information. To apply these methods in 3D deformation capture, extra machine learning technologies are needed to map the sensor data from a low-dimensional space to a higher-dimensional space [5, 21, 22, 72, 98]. However, machine learning models rely on a large volume of data for training, and finetuning models for different users also require extra personalized data. In practice, constructing a large-scale dataset is very time-consuming, and voluminous data is unavailable in many scenarios.

IMU sensors are able to acquire the 3D orientation data directly. In this paper, we adopt a self-sensing IMU sensor network to achieve 3D deformation capture. Current works mainly focus on the form factor of linear or planar structures, while the 3D deformation capture is still relatively unexplored. Our goal is to improve the accuracy and robustness of 3D deformation capture using an IMU sensor network.

2.3 Computational Fabrication of 3D Electronics

Recent advances in additive manufacturing technologies have enabled the integration of 3D forms and electronics for embedding interactions in customized designs. Prior works [29, 30, 88, 105] focused on fabricating flat electronic pieces and morphing them into 3D shapes. For example, MorphingCircuit [88] utilized 4D printing thermoplastics to create highly complex rigid circuit board. Thermoformed Circuit Borads [29] employed the

thermoforming of 3D printed plastics to construct rigid and highly conductive freeform circuit boards. These techniques support the rapid fabrication of 3D circuit boards. Unfortunately, the flexibility of sensing function is limited by the rigidity of the materials or mediums used in these works, while studies [84, 87] on the flexible prototyping based on 3D printing rarely explore the integration of electronics.

In the field of wearable technologies, embedding circuits on flexible media or placing circuits on skin surface directly enhances the flexibility of sensing [42, 51, 61, 63, 65, 68, 69]. For example, FabHandWear [65] created an end-to-end pipeline from design to fabrication of hand wearables, which supported to create customized and functional hand wearable templates. SensorKnit [63] proposed textile sensors to exploit resistive, piezoresistive, and capacitive properties of various textile structures. BodyStylus [68] provided a computer-assisted approach for on-body design and fabrication of epidermal interfaces. Most of these methods support linear or planar sensing, yet perception in 3D space is limited. Additionally, most wearable electronics are usually designed for relatively small body areas and regions [62]. We aim to improve the flexibility of 3D electronics and buildup spatial perceptual capability of flexible electronics in a larger region.

2.4 Reconfigurable Sensor Network

Researches on the reconfigurable sensor network can be divided into two categories: the wireless sensor network and the wired sensor network. The former focuses on environment monitoring applications in vast spaces, such as pollution prevention [46], agriculture [50], and structure health monitoring [58]. Our study falls into the latter category, which pays more attention to applications on finer-grained object deformation capture [14, 21, 31, 55, 79], interactive media [23, 66, 74], and flexible electronics for human wearables [45, 54, 90], etc. For example, SensorTape [14] built a modular and programmable IMU sensor network in a tape to perform twist and bend sensing. Mittendorfer et al. [55] designed skin patches based on a 3-axis accelerometer and assigned these patches in a dense layout to reconstruct 3D surfaces according to their shapes, sizes and layouts. SensorNets [90] presented an electronic skin that could integrate with reconfigurable multimodal sensor networks and be capable of sensing and responding to a variety of stimuli simultaneously. In these studies, reconfigurable sensor networks are usually built by developing modular sensor nodes. We also adopt this common scheme in this paper.

3 METHOD OVERVIEW

In this paper, we present a configurable self-sensing IMU sensor network to capture 3D deformation. The sensor network measures its own deformation and reconstructs the local shape changes during deformation. To construct such a sensor network, we develop modular IMU sensor nodes and design an origami-inspired customized pipeline. The pipeline can be regarded as a 3D–2D–3D digital–physical transition process. Firstly, we utilize an optical measurement system to obtain the 3D digital model of the shape to be measured, which offers the shape-associated geometric prior. Secondly, we simplify and unfold the 3D model into a 2D planar mesh model using a graph theory-based method. Thirdly, we fabricate the planar meshes by laser-cutting the 2D planar mesh model. This is also a digital-physical transition process. Fourthly, we assemble the fabricated planar meshes with the IMU sensor nodes to construct a customized 3D sensor network, which is a 2D-3D restoration process.

Based on the customized 3D sensor network, both the global movements and the fine-grained deformations could be reconstructed with our proposed robust self-sensing algorithm. Our algorithm proposes a novel kinematic chain model based on the four-bar linkage to describe the minimum deformation process between two adjacent sensor nodes in the sensor network. With this model, the relative spatial positions of two adjacent sensor nodes can be estimated based on three geometric prior knowledge. Finally, the locations of all sensor nodes in the sensor network are calculated through the optimal update path. Thus we can reconstruct the full deformations of a 3D shape with further interpolation.

In the following sections, we provide detailed descriptions on the hardware design (Section 4), the customized construction pipeline (Section 5), and the self-sensing algorithm of the sensor network (Section 6). We evaluate the performance of our sensor network through three experiments (Section 7). Finally, we discuss the applications and limitations of our method (Section 8).

4 HARDWARE DESIGN OF SENSOR NETWORK

4.1 Sensor Network Architecture

The architecture of the proposed sensor network is shown in Fig. 1(a). The network consists of a master node and a set of slave sensor nodes. The master is composed of a microcontroller unit (MCU) and a bluetooth low energy (BLE) module. It requests orientation data from all slave sensor nodes by a software inter-integrated circuit (I^2C) bus and sends them to the PC in real-time. Each slave is designed as a modular sensor node and consists of an MCU and an IMU sensor. The slave node is responsible to sample orientation data from an IMU sensor through a hardware I^2C bus and transmit the data to the master node in the quaternion format.

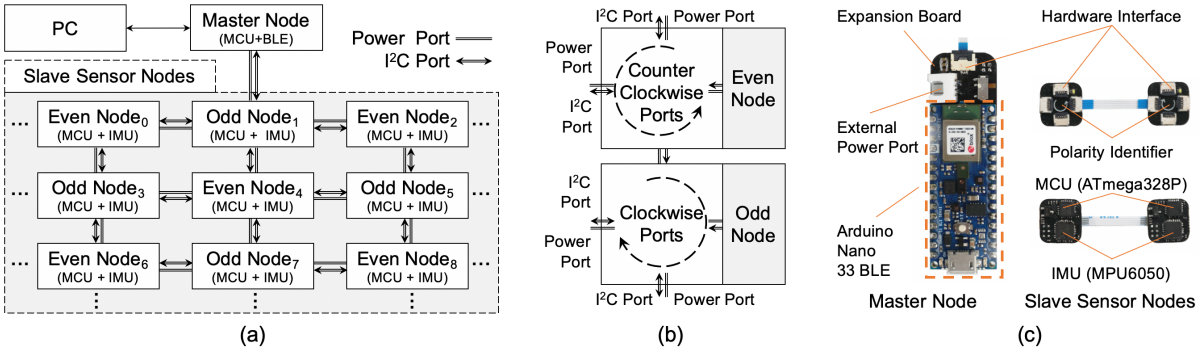

Fig. 1. (a) The architecture of the sensor network. (b) The illustration of the two types of hardware interfaces in sensor nodes. (c) The prototype of the hardware.

4.2 Hardware Interface Design

To ensure a standardized and efficient sensor network construction process, we design two types of sensor nodes with different hardware interfaces based on wired connection. We adopt the wired connection instead of the wireless communication in the sensor network to reduce the cost of components and the size of the printed circuit board (PCB) of a sensor node. Such a design supports a dense layout of the sensor network with a lightweight using experience. In practice, it is necessary to design a network with low cost and small size to support high resolution and wide range of sensing.

However, using wired connection in the sensor network results in the problem that we can not connect two nodes randomly when all sensor nodes have the same hardware interface. This is because both the power and I^2C ports have inherent polarities in physical connections. Therefore, we design two types of sensor nodes: the even node with counter clockwise ports and the odd node with clockwise ports (Fig. 1(b)). An even node is assigned an even number and an odd node is assigned an odd number in our network. The I^2C address of each sensor node is hardcoded with its own number. Therefore, two random nodes equipped with opposite polarity or parity in the sensor network can be connected.

4.3 Hardware Implementation

In the sensor network, we use an open-source electronic prototyping platform (Arduino Nano 33 BLE) with a BLE (nRF52840) module as the master node. As shown in Fig. 1(c), an expansion board is designed for the master node to support wired connection with slave sensor nodes. Meanwhile, we design modular and compact IMU sensor nodes with two types of hardware interfaces as the slave sensor nodes, the size of which is $1cm*1cm*0.1cm$. Specifically, the slave sensor node includes an MCU (ATmega328P) and an IMU sensor (MPU6050). The IMU consists of a 3-axis accelerometer and a 3-axis gyroscope. The sampling rate of IMU signals is $30Hz$. In addition, different polarity identifiers in IMU sensor nodes represent different hardware interfaces. Each sensor node has four same hardware interfaces to support multiple connections. The required orientation data in the quaternion format comes from the IMU's internal digital motion processor (DMP), which has built-in filtering and compensation algorithm. We calibrate all IMU sensor nodes. During the test, despite the lack of a magnetometer, there is no obvious data drift after one hour of static operation.

5 CUSTOMIZED CONSTRUCTION PIPELINE OF SENSOR NETWORK

We introduce origami-inspired thinking [35] to achieve a rapid and efficient customized construction pipeline of 3D sensor networks. Origami-inspired design constructs 3D functional structures from 2D planar structures, while reversely morphs 3D structures into planar structures [13, 35, 57, 67]. Motivated by this thinking, we regard the customized construction pipeline of 3D sensor networks as a 3D–2D–3D digital–physical transformation process, which is composed of 3 main steps and 7 substeps. We take the process of customizing a wearable 3D sensor network for an arm to illustrate the proposed construction pipeline intuitively (Fig. 2).

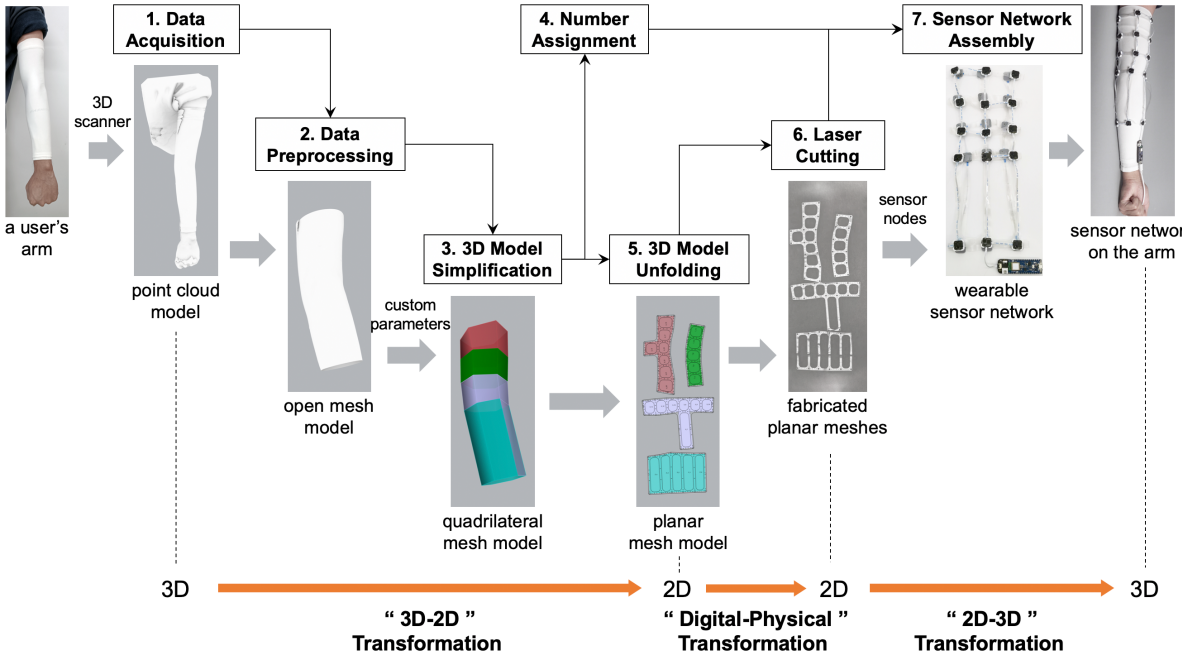

Fig. 2. The customized construction pipeline of a wearable 3D sensor network for an arm.

In the process of 3D-2D transformation, we unfold the complex 3D model scanned from the arm into simple 2D shapes. This process supports us to use more time-saving and inexpensive methods to fabricate our prototype. We select the laser cutting technology to perform a rapid digital–physical fabrication process.

In the process of 2D-3D transformation, we assemble 2D fabricated planar meshes with IMU sensor nodes to construct a customized sensor network. Because the 2D planar meshes contain the shape-associated geometric prior knowledge, the restored sensor network can fit the arm well.

The 3D model simplification determines the numbers and locations of sensor nodes placed on the arm surface. The vertices of the 3D quadrilateral mesh model in the digital space correspond to the sensor nodes of the 3D wearable sensor network in the physical space. The quadrilateral meshes represent the geometric constraints. Thus, the fabricated planar meshes provide the corresponding position constraints for sensor nodes to ensure accurate measurement of arm surface deformations.

5.1 Data Acquisition and Preprocessing

We use an optical measurement system, EinScan Pro 2X Plus[1] , to scan the measured object (e.g., a person's arm) and obtain its point cloud model, which contains the shape and size of the object. We intercept a part from the point cloud model, which corresponds to the deployment area of the sensor network on the arm. Then the remaining point cloud model is denoised and smoothed, and imported into a 3D modeling software, Rhinoceros, to be converted into an open mesh model.

5.2 3D Model Simplification

We further simplify the open mesh model into a 3D quadrilateral one with N vertices in Rhinoceros, where N vertices denote N sensor nodes in the final sensor network. The quadrilateral mesh ensures that the directions of edges in the following fabricated planar meshes can be aligned with the motion directions naturally. Each vertex in the quadrilateral mesh model contains a position vector and a normal vector. Therefore, the 3D quadrilateral mesh model provides the initial positions and orientations of all sensor nodes deployed on the arm, which serve as the shape-associated geometric prior knowledge for the subsequent deformation capture.

The total number of sensor nodes and the minimum distance between two adjacent sensor nodes are customizable parameters to fulfill different application demands. For example, reducing the number of sensor nodes to reduce the energy consumption and hardware cost; increasing the density of sensor nodes to improve the capture resolution.

5.3 Number Assignment

We assign numbers to vertices of the 3D quadrilateral mesh model to guide the subsequent assembly. Firstly, we build a connected and undirected graph $G(V, E)$ from the 3D quadrilateral mesh model. The graph $G(V, E)$ contains a vertex set V and an edge set E. The vertex $V_i \in V$ represents the i-th sensor node, and the edge $E_{i,j} \in E$ represents the adjacent relation of two sensor nodes V_i and V_j.

The operation of assigning numbers to sensor nodes is based on the breadth-first search algorithm [4], and it automatically assigns the numbers with opposite parity for each pair of adjacent nodes. Specifically, we randomly select a vertex as the root node and allocate its parity. Starting at the root node, we traverse the rest of nodes layer by layer. Nodes at the same layer are assigned the same parity and the others at the adjacent layer are assigned the opposite parity. In this way, we assign the numbers for all nodes from 1 to N in order according to their parity labels.

[1]https://www.einscan.com/

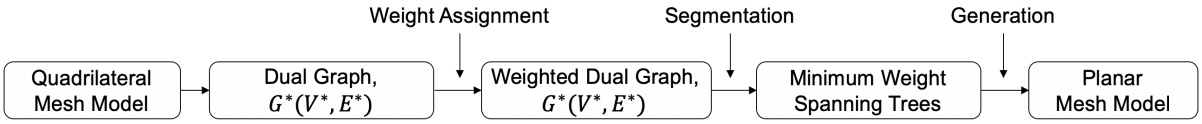

Fig. 3. The process of 3D model unfolding.

5.4 3D Model Unfolding

3D model unfolding transforms the 3D quadrilateral mesh model into a 2D planar mesh model, which facilitates applying the laser cutting technology to fabricate a 3D sensor network rapidly and efficiently.

Current studies mainly segment and unfold 3D meshes based on the irregular polyhedral or triangles [26, 59, 86, 93]. However, the segmented planar meshes obtained by these methods are usually numerous and irregular in shape, which leads to a complex and difficult fabrication and assembly process. Therefore, they are not applicable to the construction of 3D sensor networks. To solve this problem, we use quadrilateral mesh to represent a 3D model (Section 5.2).

We adopt the Kruskal's minimum spanning tree algorithm [41] to unfold a 3D quadrilateral mesh into planar meshes and minimize the number of planar meshes to simplify the fabrication and assembly process. The process of 3D model unfolding is shown in Fig. 3.

Firstly, we create the dual graph $G^*(V^*, E^*)$ from the 3D quadrilateral mesh model. In the graph $G^*(V^*, E^*)$, the node $V_i^* \in V^*$ represents the i-th quadrilateral plane of the original 3D mesh and each edge $E_{i,j}^* \in E^*$ represents the adjacent relation between two quadrilateral planes V_i^* and V_j^*.

Secondly, we assign a weight to each edge in the graph G^* based on the distance between the centroids of its two adjacent quadrilateral planes. By dividing a quadrilateral into two disjoint triangles, the centroid C of a quadrilateral can be calculated according to the centroid O_i and the area S_i of the two triangles:

$$C = \frac{\sum(S_i \cdot O_i)}{\sum S_i} \tag{1}$$

Thus, the weight W_{edge} between two adjacent quadrilateral planes with the centroid C_i and C_j is defined as:

$$W_{edge} = \left|\overrightarrow{C_i C_j}\right| \tag{2}$$

Thirdly, we use the Kruskal's minimum spanning tree algorithm to segment the weighted dual graph G^* into a minimum weight spanning tree connecting all vertices. Subsequently, we split the tree into several subtrees based on whether the weight of an edge is larger than the next edge in the tree hierarchy. Specifically, if the weight deviation of two edges on adjacent layers is greater than the preset maximum edge weight deviation in the tree and the number of nodes in a subtree is greater than the preset minimum value, the edge with a larger weight would be removed. Therefore, a series of minimum weight spanning trees are obtained. This strategy ensures small quadrilateral planes to be retained as much as possible while large quadrilateral planes to be split out. Retaining small quadrilateral planes as much as possible is helpful to simplify the assembly process of sensor network.

Finally, we can produce a planar mesh model from the original 3D quadrilateral mesh according to the structure of the minimum weight spanning trees. Our 3D model unfolding method ensures the obtained planar mesh model to maintain original geometric characteristics of the 3D mesh model.

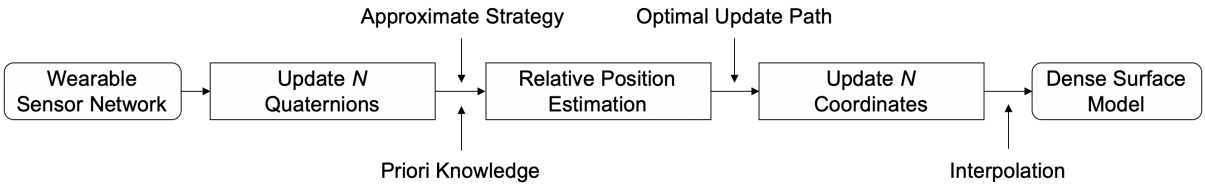

Fig. 4. The workflow of the self-sensing algorithm for deformation capture.

5.5 Laser Cutting and Sensor Network Assembly

We choose a flexible, translucent and weakly elastic clothing material, the thermoplastic polyurethane (TPU) fabric, to fabricate the planar meshes. These planar meshes can be quickly fabricated by laser cutting the planar mesh model in a few minutes. The final fabricated planar meshes provide the corresponding position and motion constraints for all sensor nodes to ensure accurate measurement of 3D deformations, and details are explained in Section 6.2. Then, the 3D sensor network can be obtained by assembling the fabricated planar meshes with the numbered IMU sensor nodes. The final result in Fig. 2 shows the case of wearing the sensor network on an arm.

6 SELF-SENSING PRINCIPLE OF SENSOR NETWORK

The 3D sensor network is used to reconstruct complex geometric deformations primarily by sensing its own deformation. We propose a robust self-sensing algorithm to reconstruct both global movements and fine-grained 3D deformations via an IMU sensor network. Our method supports a reliable, accurate, and real-time self-sensing of sensor networks by two main procedures: 1) Relative position estimation based on the geometric prior knowledge. 2) Sensor nodes' coordinates update based on the optimal update path. The complete workflow of the self-sensing algorithm for deformation capture is shown in Fig. 4.

6.1 Sensor Data Representation

To avoid the gimbal lock problem [27] in Euler angle representation, our IMU sensor network outputs the 3D orientation data in the quaternion representation. The quaternion q is a four-dimensional complex number and is usually used to represent a 3D rotation. A quaternion q can be described as $[x, y, z, w]$, where the x, y and z define the direction of rotation, and the w indicates the degree of rotation. In our method, the sensor network with N sensor nodes update N quaternions at the sampling rate of $30Hz$.

6.2 Relative Position Estimation

The relative position estimation is to calculate the relative spatial position between adjacent sensor nodes in a sensor network. We propose a novel kinematic chain model based on the four-bar linkage to represent a minimum deformation unit and achieve the relative position estimation. Since the IMU sensor only captures the orientation information, it cannot be used to measure spatial distance directly. Therefore, we introduce three geometric prior knowledge to assist the sensor network in reconstructing the minimum deformation unit.

- **The prior knowledge P1**: The planar meshes are made from a kind of weakly elastic and flexible material (TPU). Therefore, we assume that the "connection distance", rather than the spatial distance, between adjacent sensor nodes on planar meshes would remain constant under any deformation.
- **The prior knowledge P2**: The planar meshes maintain the geometric characteristics of the 3D mesh model and provide the specific movement constraints for the sensor network. Restricted by the degree of freedom of the local geometric deformation, we assume that the planar mesh connecting two sensor nodes can only perform single-degree-of-freedom motions and would be shaped as an arc in most cases.

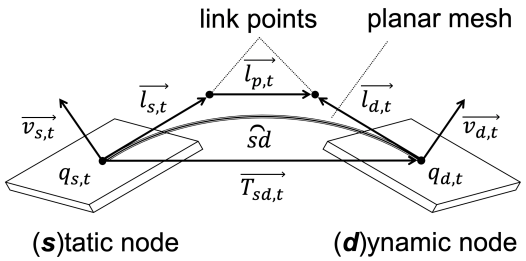

Fig. 5. The kinematic chain model represents a minimum deformation unit.

- **The prior knowledge P3**: The planar meshes simplified from the 3D quadrilateral mesh model provide the kinematic chain model with the shape-associated geometric prior knowledge, including the initial relative positions and orientations of all sensor nodes in the sensor network.

Based on three prior knowledge, we propose a novel kinematic chain model based on the four-bar linkage to represent a minimum deformation unit. The IMU sensor network provides the orientation information as the posteriori knowledge. The kinematic chain model fuses the geometric prior knowledge and the real-time updated posteriori knowledge to accurately estimate the relative spatial positions between adjacent sensor nodes.

The kinematic chain model representing a minimum deformation unit is shown in Fig. 5. In this model, a static node $\boldsymbol{s}$ and a dynamic node $\boldsymbol{d}$ are connected together by the planar mesh, which is denoted as the $\widehat{sd}$. The static node $\boldsymbol{s}$ has the known fixed position and the dynamic node $\boldsymbol{d}$ has the unknown dynamic position. We define two link points between two nodes to establish the relation of a four-bar linkage. We denote the four-bar linkage relation using the link vector $\overrightarrow{l_{s,t}}$, $\overrightarrow{l_{p,t}}$ and $\overrightarrow{l_{d,t}}$ respectively. The magnitude of $\overrightarrow{l_{s,t}}$ is equal to the magnitude of $\overrightarrow{l_{d,t}}$. The orientations of two nodes are denoted by the quaternion $q_{s,t}$ and $q_{d,t}$, as well as the unit normal vectors $\overrightarrow{v_{s,t}}$ and $\overrightarrow{v_{d,t}}$. The spatial relation between two nodes can be represented by a transformation vector $\overrightarrow{T_{sd,t}}$. The variable t represents different moments during the deformation process.

Thus, we have the following three deductions based on the kinematic chain model and three prior knowledge.

- **Based on the prior knowledge P1**, we propose an approximate strategy to improve the accuracy and robustness of our algorithm. Specifically, we use $\overrightarrow{l_{p,t}}$, $\overrightarrow{l_{s,t}}$ and $\overrightarrow{l_{d,t}}$ to approximately represent the $\widehat{sd}$, so the sum of the magnitudes of $\overrightarrow{l_{p,t}}$, $\overrightarrow{l_{s,t}}$ and $\overrightarrow{l_{d,t}}$ remain as a known constant L.
- **Based on the prior knowledge P2**, when the node $\boldsymbol{s}$ and $\boldsymbol{d}$ are parallel, the $\widehat{sd}$ becomes a semicircle. It is certain that the magnitude of $\overrightarrow{l_{p,t}}$ should be equal to the diameter of the semicircle $\widehat{sd}$, which is equal to $2L/\pi$. Thus, the magnitudes of $\overrightarrow{l_{s,t}}$ and $\overrightarrow{l_{d,t}}$ can be derived as $(L - 2L/\pi)/2$.
- **Based on the prior knowledge P3**, the initial orientations, including $\overrightarrow{v_{s,0}}$, $\overrightarrow{v_{d,0}}$ and $q_{s,0}$, $q_{d,0}$, are given, and the initial positions of the node $\boldsymbol{s}$ and $\boldsymbol{d}$ can also be obtained to calculate the initial transformation vector $\overrightarrow{T_{sd,0}}$ and the reference link vectors, $\overrightarrow{l_{s,r}}$ and $\overrightarrow{l_{d,r}}$, which represent the link vector $\overrightarrow{l_{s,t}}$ and $\overrightarrow{l_{d,t}}$ respectively in the horizontal state and the positive direction. The $\overrightarrow{l_{s,r}}$ and $\overrightarrow{l_{d,r}}$ are both static vectors. Here we define the initial time as $t = 0$.

To obtain the reference link vectors $\overrightarrow{l_{s,r}}$ and $\overrightarrow{l_{d,r}}$, we need to obtain the initial link vector $\overrightarrow{l_{s,0}}$ and $\overrightarrow{l_{d,0}}$. Take the calculation of $\overrightarrow{l_{s,0}}$ as an example, we need to calculate the projection vector $\overrightarrow{V_p}$ of the initial transformation vector

$\overrightarrow{T_{sd,0}}$ onto the $\overrightarrow{v_{s,t}}$, as shown below:

$$\overrightarrow{V_p} = (\overrightarrow{T_{sd,0}} \cdot \overrightarrow{v_{s,0}}) \times \overrightarrow{v_{s,0}} \tag{3}$$

The vector $\overrightarrow{l_{s,0}}$ can be calculated as:

$$\overrightarrow{l_{s,0}} = \frac{\overrightarrow{T_{sd,0}} - \overrightarrow{V_p}}{\left|\overrightarrow{T_{sd,0}} - \overrightarrow{V_p}\right|} \times \left|\overrightarrow{l_{s,0}}\right| \tag{4}$$

Then, the rotation of a node relative to its horizontal state in the positive direction can be represented by the real-time quaternion vector from the IMU sensor. Based on the known initial link vector $\overrightarrow{l_{s,0}}$, the reference link vectors $\overrightarrow{l_{s,r}}$ can be reversely calculated as:

$$\overrightarrow{l_{s,r}} = q^*_{s,0} \cdot \overrightarrow{l_{s,0}} \tag{5}$$

Where $q^*_{s,0}$ represents the inverse of the quaternion $q_{s,0}$. The vector $\overrightarrow{l_{d,r}}$ can also be calculated based on the above process accordingly. The reference link vectors $\overrightarrow{l_{s,r}}$ and $\overrightarrow{l_{d,r}}$ are both static vectors, never changing with nodes moving and rotating. So we can reverse above calculation process to derive the transformation vector $\overrightarrow{T_{sd,t}}$ in any moment. At the moment $\boldsymbol{t}$, the link vector $\overrightarrow{l_{s,t}}$ and $\overrightarrow{l_{d,t}}$ can be derived as:

$$\overrightarrow{l_{s,t}} = q_{s,t} \cdot \overrightarrow{l_{s,r}} \tag{6}$$

$$\overrightarrow{l_{d,t}} = q_{d,t} \cdot \overrightarrow{l_{d,r}} \tag{7}$$

Where $q_{s,t}$ and $q_{d,t}$ come from IMU sensors directly. Then, the transformation vector $\overrightarrow{T_{sd,t}}$ can be figured out:

$$\overrightarrow{T_{sd,t}} = (1 + \frac{\left|\overrightarrow{l_{p,t}}\right|}{\left|\overrightarrow{l_{s,t}} - \overrightarrow{l_{d,t}}\right|})(\overrightarrow{l_{s,t}} - \overrightarrow{l_{d,t}}) \tag{8}$$

Finally, given the coordinate $(s_{x,t}, s_{y,t}, s_{z,t})$ of the static node $\boldsymbol{s}$, the real-time coordinate $(d_{x,t}, d_{y,t}, d_{z,t})$ of the dynamic node $\boldsymbol{d}$ can be derived directly by the transformation vector $\overrightarrow{T_{sd,t}} = (\triangle_{x,t}, \triangle_{y,t}, \triangle_{z,t})$ as follows.

$$\begin{cases} d_{x,t} = s_{x,t} + \triangle_{x,t} \\ d_{y,t} = s_{y,t} + \triangle_{y,t} \\ d_{z,t} = s_{z,t} + \triangle_{z,t} \end{cases} \tag{9}$$

6.3 Coordinates Update

In the process of coordinates update, the measurement error of each kinematic chain model in sensor network would be accumulated step by step. To enhance the universality of our method, we introduce the optimal update path to overcome the cumulative errors. Our method is to minimize the error cumulation number while updating all nodes' coordinates. We firstly use the exhaustive method to acquire all the spanning trees from the aforementioned graph $G(V, E)$ (Section 5.3) as different update paths. The root node of a spanning tree is set as the starting point of an update path. Therefore, the number of error cumulation times K can be denoted as the sum of the distances among the root node n_0 and all the other nodes n_i:

$$K = \sum Distance(n_0, n_i) \tag{10}$$

The spanning tree with the minimum K would be set as the optimal update path and used for the final coordinates update. Finally, we could obtain the coordinates of all sensor nodes. It is possible to reconstruct a dense 3D model with more fine-grained geometric information by further interpolation. This 3D model can be used to represent the whole 3D deformations in real time.

7 EXPERIMENT SETUP AND RESULTS

In this section, three experiments are conducted to validate the performance of our method, including the 3D curve deformation capture, the 3D surface deformation capture, and the arm motion and deformation capture respectively.

7.1 Experimental Setup

We use a 3D printer to print different shapes of 3D models to conduct the 3D curve and 3D surface deformation capture experiments. These printed 3D models serve as the 3D objects to be measured and the original virtual 3D models serve as the ground truth. The customized sensor network measures the shape of a printed 3D models and output the coordinates of sensor nodes to reconstruct a 3D virtual model. Therefore, the differences between the original 3D model and the reconstructed 3D model indicate the performance of our method, and the smaller differences indicate the higher deformation capture accuracy.

The evaluation on deformation capture is to compare the difference when the measuring object changes from the start shape to the destination shape from one moment to another. In our experiments, the printed 3D models are fixed and inflexible, and cannot be reshaped. Therefore, the destination shape is set to be the same as the start shape, and a series of deformations will be added into the intervals from the start moment to the destination moment, which ensures the effectiveness of the evaluation. Although our evaluation method based on the 3D printing cannot evaluate the real-time differences between the measurement value and the ground truth, we focus on the evaluation of the same shape in different moments while considering deformation adequately. Such an evaluation process can achieve the same evaluation effects as the optical measurement-based methods do while effectively saving time.

We also conduct an experiment on arm motion and deformation capture to validate the performance of our method in practical applications. In this experiment, we use the aforementioned optical measurement system to capture and reconstruct the motions and deformations of a person's arm. The optical reconstructed results serve as the ground truth. We compare the ground truth and the 3D arm model reconstructed by our sensor network to obtain the final evaluation results.

7.2 3D Curve Deformation Capture

A conical spiral model (Fig. 6(a)) in the length of $1015mm$ is printed to conduct this experiment. A network with 30 IMU sensor nodes (Fig. 6(b)) is constructed to capture the deformation of the 3D curve. Since the curve's geometry is simple, all the sensor nodes are assigned directly to a straight-line model with the same length. Then the planar mesh of the line model is obtained by laser cutting and the sensor network is assembled quickly. The complete fabrication and assembly process takes about 10 minutes.

We measure the deformation process in which the 30 sensor nodes deform from a straight line into a conical spiral. This measurement process is conducted 10 times by repeatedly folding and unfolding the sensor network. Fig. 6(c) shows the virtual conical spiral model reconstructed by the sensor network. The final average evaluation results for 10 times are shown in Table 2 (Section 7.5), including the average error ($6.15mm$), the maximum error ($15.25mm$), the root mean square (RMS) error ($7.07mm$) and the average error rate (2.42%).

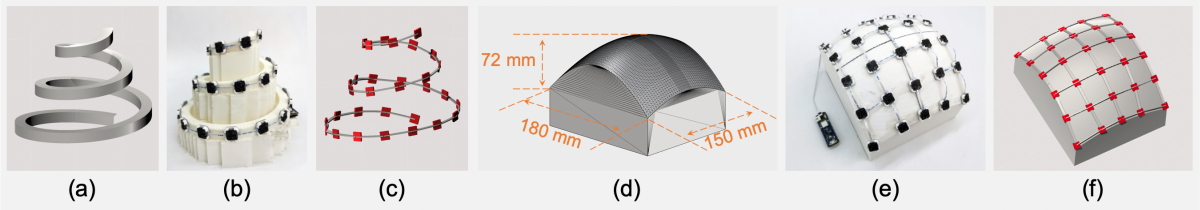

Fig. 6. (a) The 3D model of a conical spiral. (b) The 3D printed model of a conical spiral attached with the sensor network. (c) The virtual model reconstructed by the sensor network. (d) The 3D model of a rotational paraboloid. (e) The 3D printed model of a rotational paraboloid attached with the sensor network. (f) The virtual model reconstructed by the sensor network.

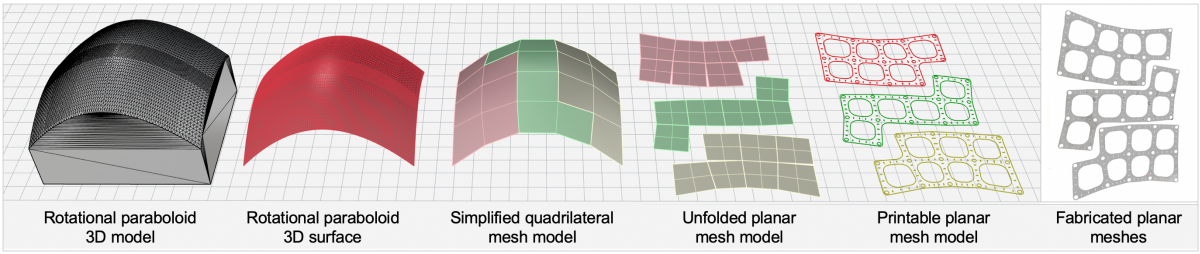

Fig. 7. The results of model simplification, unfolding and fabricating.

7.3 3D Surface Deformation Capture

A rotational paraboloid model (Fig. 6(d)) in the size of $180mm150mm72mm$ is printed to conduct this experiment. A network with 30 IMU sensor nodes (Fig. 6(e)) is constructed to capture the deformation of the 3D surface. Fig. 7 shows the customization pipeline of model simplification, unfolding and fabricating respectively. The complete fabrication from cutting to assembling takes about 20 minutes. Fig. 6(f) shows the virtual rotational paraboloid model reconstructed by the sensor network. Especially, the assembled 3D meshes instead of the cables in the sensor network constrain the motions of sensor nodes.

To evaluate the accuracy of the sensor network, we conduct static and dynamic experiments respectively. The static experiment measures the initial shape without any motion and deformation. The dynamic experiment measures the final results of the sensor network after a series of deformations. Fig. 8(a) shows the detailed deformation process in the dynamic experiment, which contains 5 steps. Fig. 8(b) shows the corresponding virtual models reconstructed by the sensor network in 5 steps. It can be seen that our method accurately reconstructs the deformed model in the case of various complex deformations.

After calculating the coordinates of all sensor nodes, the radial basis function (RBF) interpolation algorithm [91] is applied to produce more points, which facilitates reconstructing a denser rotational paraboloid (Fig. 9). The error comparison and analysis are carried out between the reconstructed rotational paraboloid and the original rotational paraboloid model in a 3D point cloud processing software, CloudCompare[2].

We repeat the measurement 10 times by following the folding and unfolding sequence in Fig. 8(a). The final average evaluation results for 10 times are shown in Table 2 (Section 7.5), including the average error (static: $4.22mm$, dynamic: $3.90mm$), the maximum error (static: $8.75mm$, dynamic: $8.43mm$), the RMS error (static: $4.55mm$, dynamic: $4.29mm$) and the average error rate (static: 1.71%, dynamic: 1.63%). The detailed error comparisons of

[2]https://cloudcompare.org/

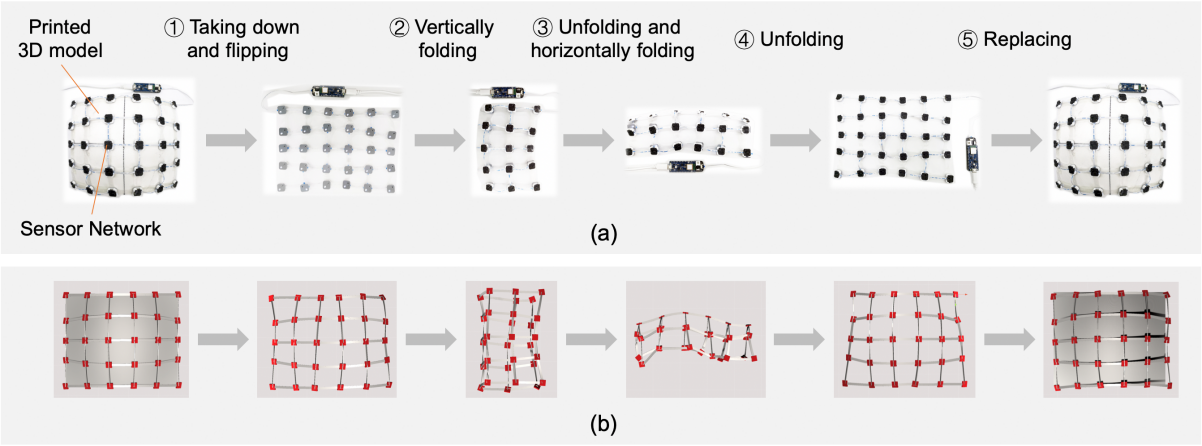

Fig. 8. A series of deformations on the sensor network. (b) The corresponding virtual model reconstructed by the sensor network.

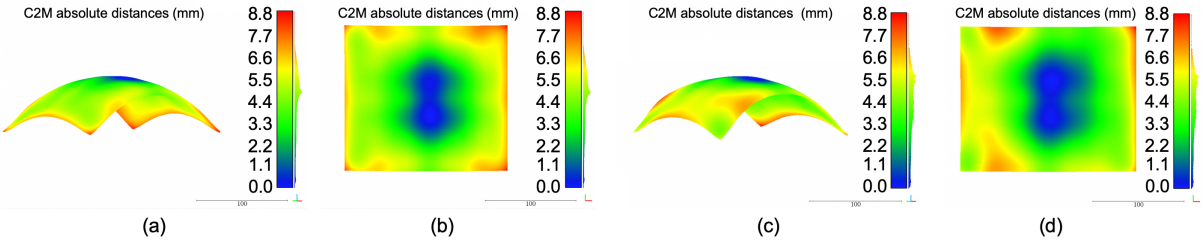

Fig. 9. Interpolated dense rotational paraboloid model and the details of error comparison in static and dynamic conditions. Colors that tend toward blue have smaller errors. The "C2M" in the figures is the abbreviation of " Cloud to Mesh". (a) oblique view in the static condition. (b) vertical view in the static condition. (c) oblique view in the dynamic condition. (d) vertical view in the dynamic condition.

the static and dynamic experiments are shown in Fig. 9. Here, the results in the static condition are shown in Fig. 9(a) and Fig. 9(b) and the results in the dynamic condition are shown in Fig. 9(c) and Fig. 9(d). The colors that tend toward blue have smaller errors. It is clear that our method can accurately reconstruct the 3D surface deformation with no more than $1cm$ error.

7.4 Arm Motion and Deformation Capture

A customized wearable sensor network containing 30 IMU sensor nodes is constructed to conduct the arm motion and deformation capture experiment (Fig. 10(a)). The complete fabrication and assembly process takes about 25 minutes (Fig. 2). We use an optical measurement system to evaluate the arm test prototype in different bending angles. The deformation process is presented in Fig. 10(a) from left to right. Fig. 10(b) shows the reconstructed virtual arm models. Fig. 10(c) shows the interpolated dense arm models and the details of error comparison.

We repeat the experiment 10 times by following the deformation process in Fig. 10(a), and then calculate the average results for different bending angles in these 10 experiments. As shown in Table 2 (Section 7.5), the

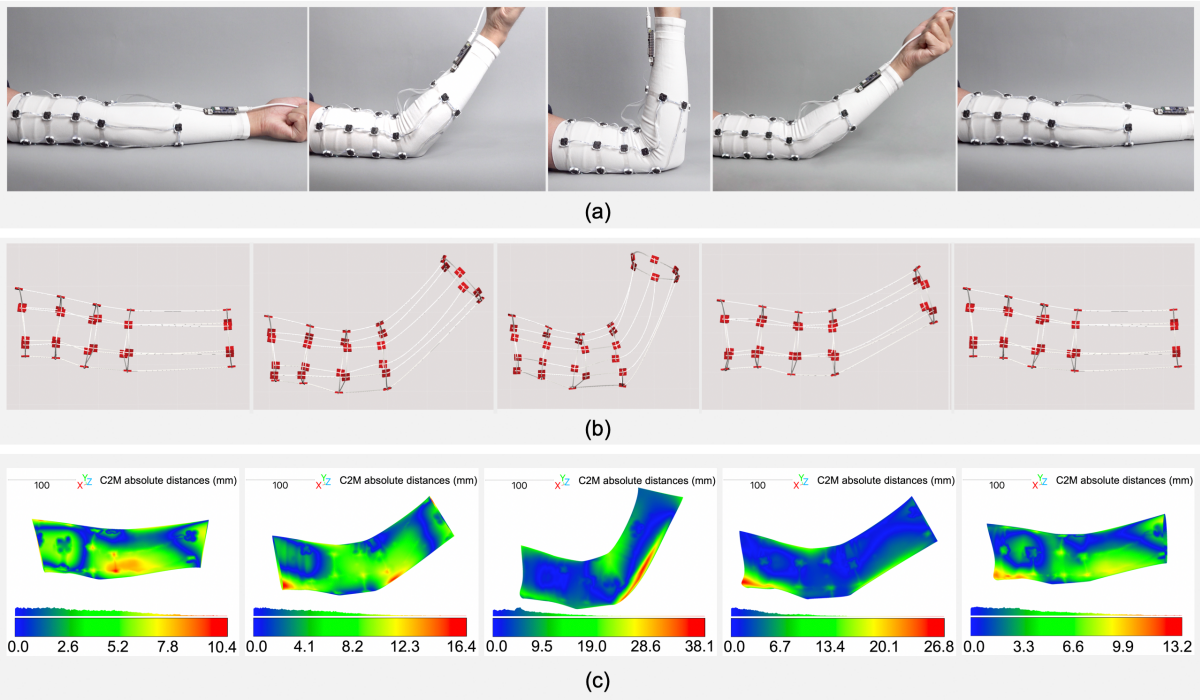

Fig. 10. (a) Arm test prototypes in different bending angles. (b) Reconstructed virtual arm models in different bending angles. (c) the interpolated dense arm model and details of error comparison in different bending angles. Colors tend to blue have smaller errors.

average error is 4.59*mm*, the maximum error is 21.00*mm*, the RMS error is 5.88*mm* and the average error rate is 1.40%.

Fig. 10(c) shows the detailed evaluation results in different bending angles. The errors are calculated by the comparison of the optical ground truth and the interpolated dense arm model. The colors that tend to blue have smaller errors. The detailed evaluation results in the five bending angles from left to right in Fig. 10(c) are as follows. The average errors are 3.26*mm*, 4.21*mm*, 7.31*mm*, 4.48*mm* and 3.71*mm* respectively, the maximum errors are 10.44*mm*, 16.37*m*m, 38.10*mm*, 26.83*mm* and 13.24*mm* respectively. These results indicate that errors increase with increasing bending angles. However, even in a challenging scenario, namely at the 90-degree bending angle, the worst average error result (7.31*mm*) is less than 1.00*cm*. The above results indicate that our method can accurately reconstruct the arm motions and deformations.

7.5 Comparison with Existing Researches

Table 2 shows the comparison results between our evaluation examples and the existing works based on different sensing methods including the capacitance [21, 79], the IMU sensor network [55], the piezoelectricity [72] and the resistance [10]. Specially, we add works on monocular 3D human pose estimation on Human3.6M dataset [33, 99] as the representative of vision-based methods. Especially, it is hard for us to reproduce all the compared methods in the experiments. Although our experimental setup is different from the existing works, the deformations

Table 2. Comparisons with Existing Researches.

Methods		Deformation Types	Average Error (mm)	Maximum Error (mm)	RMS Error (mm)	Average Error Rate (%)
Ours	conical spiral case	3D Curve	6.15	15.25	7.07	2.42
	rotational paraboloid case (static)	3D Surface	4.22	8.75	4.55	1.71
	rotational paraboloid case (dynamic)	3D Surface	3.90	8.43	4.29	1.63
	arm case	3D Surface	4.59	**21.00**	5.88	**1.40**
Capacitance (arm case) [21]		3D Surface	**3.46**	30.82	\	\
Capacitance (radii test case) [79]		3D Curve	19.03	\	\	4.16
IMU sensor network (closed loop case) [55]		3D Curve	10.46	\	\	4.71
Piezoelectricity (2.5D surface case) [72]		2.5D Surface	15.00	22.00	\	4.12
Resistance [10]		1D Curve	7.15	18.81	\	\
Monocular 3D human pose estimation on Human3.6M [33, 99]		3D Surface	39.8	\	\	\

measured in our experiments are much more complex than that measured by the most compared methods. Therefore, the comparison results can be used to verify the performance of our method.

As shown in Table 2, our method achieves the state-of-the-art performance in terms of maximum error and average error rate. Our average error is 1.13mm higher than [21], but our maximum error is 9.82mm less than its result. In summary, the comprehensive performance of our method outperforms existing methods.

7.6 Robustness Analysis

3D curve deformation capture is a challenging task because of the large cumulative error, caused by the form factor of the curve and the dynamic gained drifts from all IMU sensor nodes during motion. Refer to the equation (10) in Section 6.3, theoretically, the cumulative error of the sensor network in measuring the conical spiral model is larger than that in measuring the rotational paraboloid case and the arm case. Our experimental results show that the results in the conical spiral case (average error = 6.15mm) are not substantially higher than the results in the rotational paraboloid case (average error = 3.90mm) and the arm case (average error = 4.59mm). It shows that our method is robust and still performs well while dealing with a large cumulative error.

8 DISCUSSION AND FUTURE WORKS

8.1 New Possibility of Applications

Our method is able to accurately capture 3D deformations of various objects by quickly customizing a sensor network that matches the shape of the object. It can be applied in various emerging interactive applications. We further discuss the potential design space for three test prototypes in evaluation experiments.

- **Shape Measurement Tools**. By setting the initial shape of the sensor network to a specific shape, such as a straight line or a square plane, a shape measurement tool can be created. The sensor network needs to take the initial shape as the starting point for each measurement, then close to the surface of the measured object. The final deformation result is the measured shape of the object. Such a shape measurement tool can be used to measure the surface curvature, bending angle, angularity, profile shape and other characteristics of an object.
- **Smart Tangible User Interface**. Integrating the sensor network into the tangible user interface is one of the most important applications of our method. Our method can enhance the self-perception ability of existing tangible user interfaces, and support a more natural and free form of interaction. For example, a

smart sleep monitoring system could be developed by integrating our sensor network into pillows. The user's sleep posture can be accurately restored by capturing the pillow's surface deformation.

- **Wearable Input Devices**. Another important application is to build wearable input devices. Our sensor network can work on different human body parts such as human limbs, hands, torso and face, as long as the deformation space of the body part is large enough to place $1cm * 1cm * 0.1cm$ sensor nodes. Our method will support a wide variety of body gesture control applications in the future, such as providing accurate and fine-grained avatar manipulation to increase immersive experience in virtual reality, and reconstructing body motions and deformations to support medical rehabilitation training.

8.2 Usability of the Sensor Network

Our sensor network provides a low-cost, low-power and real-time deformation capture solution. We use low-cost hardware components to design IMU sensor nodes. The cost of a single IMU sensor node is less than $3. The average power consumption of each sensor node is about 58mW, so a 3800mAh 3.7V lithium polymer battery is enough to power a sensor network with 30 sensor nodes for 8 hours. We adopt the 7-bit addressing in the software I^2C bus to achieve the communication between the master and slave sensor nodes, thus allowing up to 128 sensor nodes to be connected simultaneously. The pull-up resistor value should be changed with the number of slave sensor nodes to keep the system running. In addition, the average update rate of IMU signals in this paper is about $30Hz$, supporting the real-time interactions of most applications.

In this paper, we only construct the sensor network with no more than 48 sensor nodes (30 in evaluation and 48 in supplementary video). For the large object deformation capture scenarios such as the measurements of full-body, where more slave sensor nodes are required, we suspect that the stability problem may occur in the communication bus. This is because I^2C is a short-distance communication protocol and is highly sensitive to capacitance changes. One solution is to set up several independent hardware subsystems, namely using multiple masters to control different slave sensor networks. This method is able to avoid long-wire connections and is still applicable to our self-sensing algorithm. Another way is to replace I^2C with differential RS485 protocol, which supports long cabling distances in electrically noisy environments. However, this approach requires incorporating additional RS485 interface IC into the hardware design, leading to an increase in component cost and PCB size of sensor nodes. In the future, we will develop an RS485-based version of the sensor node to improve system stability and extend the application scope of our sensor network.

Another work that needs to be improved in the future is the I^2C addressing scheme in our sensor network. The I^2C address of each sensor node is assigned by hardcoding. Actually, when we were hardcoding a sensor node, we manually tagged its I^2C address number on its PCB. These tags on sensor nodes would guide users on how to connect the sensor nodes in the right configuration while ensuring that their address matched their physical location. Indeed, such a manual tagging process is not very convenient, but it only occurs in the preliminary hardcoding works and does not influence the sensor network assembly process. We would like to upgrade our sensor network to a peer-to-peer network in the future, thus allowing automatic address assignment based on the physical locations of the nodes.

8.3 Necessity of Customized Fabrication Pipeline

Our customized fabrication pipeline is a 3D–2D–3D digital–physical transformation process. The core of this pipeline is to simplify and unfold complex 3D models into 2D meshes for rapid fabrication and meanwhile support efficient assembly of 2D meshes to restore 3D shapes. Such a fabrication pipeline also cooperates with our self-sensing algorithm to achieve deformation capture. Specifically, the 3D model simplification provides the algorithm with the shape-associated geometric prior knowledge, namely the prior knowledge P3. The 3D model unfolding provides the prior knowledge P2 and ensures that the fabricated planar meshes can provide motion

constraints for the sensor network while maintaining the geometric properties of the original 3D shape. Besides, the material properties of the planar meshes provide the algorithm with the prior knowledge P1. The pipeline fabricates a set of planar meshes that contain the 3D model shape information and provide motion constraints, which helps our sensor network to accurately capture the deformation process of complex 3D shapes.

Additionally, our fabrication pipeline is primarily used to convert complex 3D surfaces into 2D planes, where 3D surfaces are much more difficult to be fabricated than 2D planes. For 3D curves or simple 2D surfaces, this method is not necessarily required.

8.4 Generality of Self-sensing Algorithm

Although we use the low-cost 6-axis IMU sensors (MPU6050) to obtain orientation data, our self-sensing algorithm is compatible with any other types of 6-axis and 9-axis IMUs. In this paper, using 6-axis IMUs is to ensure immunity to magnetic interference, and thus extend the application scope. The selection of IMU sensors depends on application demands for cost, precision, etc.

8.5 Limitations on Wearing Experience

For wearable applications, although our customized sensor network could fit the human body surface well, we still feel slight constraints from the planar meshes while bending arms. This is because the fabricated planar meshes lack sufficient elasticity to accommodate the large deformations caused by elbow bending at a sharp angle. In the future, we hope to explore new fabrics to fabricate wearable meshes to enhance the flexibility of the network, and provide more comfortable wearing experiences for users.

9 CONCLUSION

In this paper, we present a configurable self-sensing IMU sensor network for complex 3D deformation capture in real time. We propose a kinematic chain model based on the four-bar linkage to describe the minimum deformation process of 3D deformations. We also introduce three geometric priors to assist the kinematic chain model in achieving robust 3D deformation capture. In addition, we design an efficient pipeline to fabricate customized 3D sensor networks for different shapes. It incorporates origami-inspired thinking and customizes a sensor network through a 3D–2D–3D digital–physical transition process. The experimental results demonstrate that our method achieves comparable performance (average error at 4.59mm, average error rate at 1.40%) with state-of-the-art methods. In summary, our method supports an accurate and reliable 3D deformation capture. We release the design files in this project at github.com/ZJUZZH/Deformation-Capture-By-IMU-Sensor-Network.

ACKNOWLEDGMENTS

This project is supported by National Key R&D Program of China (2018AAA0100703), the National Natural Science Foundation of China (No. 62202423 and No. 62002321), Zhejiang Provincial Natural Science Foundation of China under Grant No. LY23F020020, and the Fundamental Research Funds for the Central Universities (No. 2022FZZX01-22).

The authors would also like to thank all the reviewers and participants. Thank Zihan Yan, Yue Yang, Kexing Wang and Yufan Xi for constructive suggestions on the paper.

REFERENCES

[1] Morteza Amjadi, Ki-Uk Kyung, Inkyu Park, and Metin Sitti. 2016. Stretchable, Skin-Mountable, and Wearable Strain Sensors and Their Potential Applications: A Review. *Advanced Functional Materials* 26, 11, 1678–1698. https://doi.org/10.1002/adfm.201504755

[2] Hedan Bai, Shuo Li, Jose Barreiros, Yaqi Tu, Clifford R. Pollock, and Robert F. Shepherd. 2020. Stretchable distributed fiber-optic sensors. *Science* 370, 6518, 848–852. https://doi.org/10.1126/science.aba5504

[3] Ravin Balakrishnan, George Fitzmaurice, Gordon Kurtenbach, and Karan Singh. 1999. Exploring Interactive Curve and Surface Manipulation Using a Bend and Twist Sensitive Input Strip. In *Proceedings of the 1999 Symposium on Interactive 3D Graphics* (Atlanta, Georgia, USA) *(I3D '99)*. 111–118. https://doi.org/10.1145/300523.300536

[4] Alan Bundy and Lincoln Wallen. 1984. Breadth-First Search. In *Catalogue of Artificial Intelligence Tools*. 13–13. https://doi.org/10.1007/978-3-642-96868-6_25

[5] Moritz Bächer, Benjamin Hepp, Fabrizio Pece, Paul G. Kry, Bernd Bickel, Bernhard Thomaszewski, and Otmar Hilliges. 2016. DefSense: Computational Design of Customized Deformable Input Devices. In *Proceedings of the 2016 CHI Conference on Human Factors in Computing Systems (CHI '16)*. 3806–3816. https://doi.org/10.1145/2858036.2858354

[6] Francesco Caputo, Alessandro Greco, Egidio D'Amato, Immacolata Notaro, and Stefania Spada. 2019. IMU-Based Motion Capture Wearable System for Ergonomic Assessment in Industrial Environment. In *Advances in Human Factors in Wearable Technologies and Game Design*. 215–225.

[7] Vivek Chandel, Arijit Sinharay, Nasimuddin Ahmed, and Avik Ghose. 2016. Exploiting IMU Sensors for IOT Enabled Health Monitoring. In *Proceedings of the First Workshop on IoT-Enabled Healthcare and Wellness Technologies and Systems (IoT of Health '16)*. 21–22. https://doi.org/10.1145/2933566.2933569

[8] Anargyros Chatzitofis, Dimitrios Zarpalas, Petros Daras, and Stefanos Kollias. 2021. DeMoCap: Low-Cost Marker-Based Motion Capture. *International Journal of Computer Vision* 129, 12, 3338–3366. https://doi.org/10.1007/s11263-021-01526-z

[9] He Chen, Hyojoon Park, Kutay Macit, and Ladislav Kavan. 2021. Capturing Detailed Deformations of Moving Human Bodies. *ACM Trans. Graph.* 40, 4. https://doi.org/10.1145/3450626.3459792

[10] Chin-yu Chien, Rong-Hao Liang, Long-Fei Lin, Liwei Chan, and Bing-Yu Chen. 2015. FlexiBend: Enabling Interactivity of Multi-Part, Deformable Fabrications Using Single Shape-Sensing Strip. In *Proceedings of the 28th Annual ACM Symposium on User Interface Software & Technology (UIST '15)*. 659–663. https://doi.org/10.1145/2807442.2807456

[11] Hongsuk Choi, Gyeongsik Moon, Ju Yong Chang, and Kyoung Mu Lee. 2021. Beyond Static Features for Temporally Consistent 3D Human Pose and Shape From a Video. In *Proceedings of the IEEE/CVF Conference on Computer Vision and Pattern Recognition (CVPR)*. 1964–1973.

[12] Sung Yun Chung, Hwa-Jin Lee, Duck-Jae You, Sanghun Cho, Buil Nam, Tae Il Lee, and Youn Sang Kim. 2016. Piezoelectric Bending Motion Sensor for Simultaneous Detection of Bending Curvature and Speed. *ECS Transactions* 75, 16, 277–279. https://doi.org/10.1149/07516.0277ecst

[13] Erik D Demaine and Joseph O'Rourke. 2007. *Geometric folding algorithms: linkages, origami, polyhedra*. Cambridge university press.

[14] Artem Dementyev, Hsin-Liu (Cindy) Kao, and Joseph A. Paradiso. 2015. SensorTape: Modular and Programmable 3D-Aware Dense Sensor Network on a Tape. In *Proceedings of the 28th Annual ACM Symposium on User Interface Software & Technology (UIST '15)*. 649–658. https://doi.org/10.1145/2807442.2807507

[15] Ahmed Elhayek, Onorina Kovalenko, Pramod Murthy, Jameel Malik, and Didier Stricker. 2018. Fully Automatic Multi-person Human Motion Capture for VR Applications. In *Virtual Reality and Augmented Reality*. 28–47.

[16] P. Ferdinand, S. Magne, and G. Laffont. 2013. Optical fiber sensors to improve the safety of nuclear power plants. In *Fourth Asia Pacific Optical Sensors Conference*, Vol. 8924. 89242G. https://doi.org/10.1117/12.2033922

[17] Liang Gao, Gaofei Zhang, Bo Yu, Ziwei Qiao, and Junchao Wang. 2020. Wearable human motion posture capture and medical health monitoring based on wireless sensor networks. *Measurement* 166, 108252. https://doi.org/10.1016/j.measurement.2020.108252

[18] Carmelo Gentile and Giulia Bernardini. 2010. Radar-based measurement of deflections on bridges and large structures. *European Journal of Environmental and Civil Engineering* 14, 4, 495–516. https://doi.org/10.1080/19648189.2010.9693238

[19] Giada Gerboni, Alessandro Diodato, Gastone Ciuti, Matteo Cianchetti, and Arianna Menciassi. 2017. Feedback Control of Soft Robot Actuators via Commercial Flex Bend Sensors. *IEEE/ASME Transactions on Mechatronics* 22, 4, 1881–1888. https://doi.org/10.1109/TMECH.2017.2699677

[20] Nima Ghorbani and Michael J. Black. 2021. SOMA: Solving Optical Marker-Based MoCap Automatically. In *Proceedings of the IEEE/CVF International Conference on Computer Vision (ICCV)*. 11117–11126.

[21] Oliver Glauser, Daniele Panozzo, Otmar Hilliges, and Olga Sorkine-Hornung. 2019. Deformation Capture via Soft and Stretchable Sensor Arrays. *ACM Trans. Graph.* 38, 2. https://doi.org/10.1145/3311972

[22] Oliver Glauser, Shihao Wu, Daniele Panozzo, Otmar Hilliges, and Olga Sorkine-Hornung. 2019. Interactive Hand Pose Estimation Using a Stretch-Sensing Soft Glove. *ACM Trans. Graph.* 38, 4. https://doi.org/10.1145/3306346.3322957

[23] Nan-Wei Gong, Steve Hodges, and Joseph A. Paradiso. 2011. Leveraging Conductive Inkjet Technology to Build a Scalable and Versatile Surface for Ubiquitous Sensing. In *Proceedings of the 13th International Conference on Ubiquitous Computing (UbiComp '11)*. 45–54. https://doi.org/10.1145/2030112.2030120

[24] Pengfei Gui, Liqiong Tang, and Subhas Mukhopadhyay. 2015. MEMS based IMU for tilting measurement: Comparison of complementary and kalman filter based data fusion. In *2015 IEEE 10th Conference on Industrial Electronics and Applications (ICIEA)*. 2004–2009. https://doi.org/10.1109/ICIEA.2015.7334442

[25] Eunchong Ha, Gongkyu Byeon, and Sunjin Yu. 2022. Full-Body Motion Capture-Based Virtual Reality Multi-Remote Collaboration System. *Applied Sciences* 12, 12. https://doi.org/10.3390/app12125862

[26] Yue Hao, Yun-hyeong Kim, and Jyh-Ming Lien. 2018. Synthesis of Fast and Collision-Free Folding of Polyhedral Nets. In *Proceedings of the 2nd Annual ACM Symposium on Computational Fabrication (SCF '18)*. Article 2, 10 pages. https://doi.org/10.1145/3213512.3213517

[27] Evan G. Hemingway and Oliver M. O'Reilly. 2018. Perspectives on Euler angle singularities, gimbal lock, and the orthogonality of applied forces and applied moments. *Multibody System Dynamics* 44, 1, 31–56. https://doi.org/10.1007/s11044-018-9620-0

[28] Jeffrey Henderson, Joan Condell, James Connolly, Daniel Kelly, and Kevin Curran. 2021. Review of Wearable Sensor-Based Health Monitoring Glove Devices for Rheumatoid Arthritis. *Sensors* 21, 5. https://doi.org/10.3390/s21051576

[29] Freddie Hong, Connor Myant, and David E Boyle. 2021. Thermoformed Circuit Boards: Fabrication of Highly Conductive Freeform 3D Printed Circuit Boards with Heat Bending. In *Proceedings of the 2021 CHI Conference on Human Factors in Computing Systems (CHI '21)*. Article 669, 10 pages. https://doi.org/10.1145/3411764.3445469

[30] Freddie Hong, Luca Tendera, Connor Myant, and David Boyle. 2022. Vacuum-Formed 3D Printed Electronics: Fabrication of Thin, Rigid and Free-Form Interactive Surfaces. *SN Computer Science* 3, 4, 275. https://doi.org/10.1007/s42979-022-01174-1

[31] Takayuki Hoshi and Hiroyuki Shinoda. 2008. 3D shape measuring sheet utilizing gravitational and geomagnetic fields. In *2008 SICE Annual Conference*. 915–920. https://doi.org/10.1109/SICE.2008.4654785

[32] Yonghui Hu, Yong Yan, Christos Efstratiou, and David Vela-Orte. 2021. Quantitative Shape Measurement of an Inflatable Rubber Dam Using an Array of Inertial Measurement Units. *IEEE Transactions on Instrumentation and Measurement* 70, 1–10. https://doi.org/10.1109/TIM.2021.3061244

[33] Catalin Ionescu, Dragos Papava, Vlad Olaru, and Cristian Sminchisescu. 2014. Human3.6M: Large Scale Datasets and Predictive Methods for 3D Human Sensing in Natural Environments. *IEEE Transactions on Pattern Analysis and Machine Intelligence* 36, 7, 1325–1339.

[34] Useok Jeong and Kyu-Jin Cho. 2016. A Novel Low-Cost, Large Curvature Bend Sensor Based on a Bowden-Cable. *Sensors* 16, 7. https://doi.org/10.3390/s16070961

[35] Bingcong Jian, Frédéric Demoly, Yicha Zhang, H. Jerry Qi, Jean-Claude André, and Samuel Gomes. 2022. Origami-Based Design for 4D Printing of 3D Support-Free Hollow Structures. *Engineering* 12, 70–82. https://doi.org/10.1016/j.eng.2021.06.028

[36] Chengming Jiang and Jinhui Song. 2015. An Ultrahigh-Resolution Digital Image Sensor with Pixel Size of 50 nm by Vertical Nanorod Arrays. *Advanced Materials* 27, 30, 4454–4460. https://doi.org/10.1002/adma.201502079

[37] Hanbyul Joo, Hao Liu, Lei Tan, Lin Gui, Bart Nabbe, Iain Matthews, Takeo Kanade, Shohei Nobuhara, and Yaser Sheikh. 2015. Panoptic Studio: A Massively Multiview System for Social Motion Capture. In *Proceedings of the IEEE International Conference on Computer Vision (ICCV)*. 3334–3342.

[38] Robin K. Kammerlander, André Pereira, and Simon Alexanderson. 2021. Using Virtual Reality to Support Acting in Motion Capture with Differently Scaled Characters. In *2021 IEEE Virtual Reality and 3D User Interfaces (VR)*. 402–410. https://doi.org/10.1109/VR50410.2021.00063

[39] Takashi Kato, Akio Yamamoto, and Toshiro Higuchi. 2003. Shape recognition using piezoelectric thin films. In *IEEE International Conference on Industrial Technology, 2003*, Vol. 1. 112–116. https://doi.org/10.1109/ICIT.2003.1290252

[40] Muhammed Kocabas, Chun-Hao P. Huang, Joachim Tesch, Lea Müller, Otmar Hilliges, and Michael J. Black. 2021. SPEC: Seeing People in the Wild With an Estimated Camera. In *Proceedings of the IEEE/CVF International Conference on Computer Vision (ICCV)*. 11035–11045.

[41] Joseph B. Kruskal. 1956. On the Shortest Spanning Subtree of a Graph and the Traveling Salesman Problem. *Proc. Amer. Math. Soc.* 7, 1, 48–50. https://doi.org/10.2307/2033241

[42] Pin-Sung Ku, Md. Tahmidul Islam Molla, Kunpeng Huang, Priya Kattappurath, Krithik Ranjan, and Hsin-Liu Cindy Kao. 2022. SkinKit: Construction Kit for On-Skin Interface Prototyping. *Proc. ACM Interact. Mob. Wearable Ubiquitous Technol.* 5, 4. https://doi.org/10.1145/3494989

[43] Jie Li, Xiaofeng Liu, Zhelong Wang, Hongyu Zhao, Tingting Zhang, Sen Qiu, Xu Zhou, Huili Cai, Rongrong Ni, and Angelo Cangelosi. 2022. Real-Time Human Motion Capture Based on Wearable Inertial Sensor Networks. *IEEE Internet of Things Journal* 9, 11, 8953–8966. https://doi.org/10.1109/JIOT.2021.3119328

[44] Xiaodong Li, Rongwei Wen, Zhong Shen, Zheng Wang, Keith Dip Kei Luk, and Yong Hu. 2018. A Wearable Detector for Simultaneous Finger Joint Motion Measurement. *IEEE Transactions on Biomedical Circuits and Systems* 12, 3, 644–654. https://doi.org/10.1109/TBCAS.2018.2810182

[45] J. Lifton, M. Broxton, and J.A. Paradiso. 2003. Distributed sensor networks as sensate skin. In *SENSORS, 2003 IEEE*, Vol. 2. 743–747 Vol.2. https://doi.org/10.1109/ICSENS.2003.1279040

[46] Yu-Pin Lin, Hussnain Mukhtar, Kuan-Ting Huang, Joy R. Petway, Chiao-Ming Lin, Cheng-Fu Chou, and Shih-Wei Liao. 2020. Real-Time Identification of Irrigation Water Pollution Sources and Pathways with a Wireless Sensor Network and Blockchain Framework. *Sensors* 20, 13. https://doi.org/10.3390/s20133634

[47] Zhen Lin. 2021. Research on film animation design based on inertial motion capture algorithm. *Soft Computing* 25, 18, 12491–12505. https://doi.org/10.1007/s00500-021-06001-y

[48] Ruibo Liu, Qijia Shao, Siqi Wang, Christina Ru, Devin Balkcom, and Xia Zhou. 2019. Reconstructing Human Joint Motion with Computational Fabrics. *Proc. ACM Interact. Mob. Wearable Ubiquitous Technol.* 3, 1. https://doi.org/10.1145/3314406

[49] Shiqiang Liu, Junchang Zhang, Yuzhong Zhang, and Rong Zhu. 2020. A wearable motion capture device able to detect dynamic motion of human limbs. *Nature Communications* 11, 1, 5615. https://doi.org/10.1038/s41467-020-19424-2

[50] Jaime Lloret, Sandra Sendra, Laura Garcia, and Jose M. Jimenez. 2021. A Wireless Sensor Network Deployment for Soil Moisture Monitoring in Precision Agriculture. *Sensors* 21, 21. https://doi.org/10.3390/s21217243

[51] Eric Markvicka, Guanyun Wang, Yi-Chin Lee, Gierad Laput, Carmel Majidi, and Lining Yao. 2019. ElectroDermis: Fully Untethered, Stretchable, and Highly-Customizable Electronic Bandages. In *Proceedings of the 2019 CHI Conference on Human Factors in Computing Systems (CHI '19)*. 1–10. https://doi.org/10.1145/3290605.3300862

[52] Matteo Menolotto, Dimitrios-Sokratis Komaris, Salvatore Tedesco, Brendan O'Flynn, and Michael Walsh. 2020. Motion Capture Technology in Industrial Applications: A Systematic Review. *Sensors* 20, 19. https://doi.org/10.3390/s20195687

[53] Rui Min, Zhengyong Liu, Luis Pereira, Chenkun Yang, Qi Sui, and Carlos Marques. 2021. Optical fiber sensing for marine environment and marine structural health monitoring: A review. *Optics & Laser Technology* 140, 107082. https://doi.org/10.1016/j.optlastec.2021.107082

[54] Behram F.T. Mistree and Joseph A. Paradiso. 2010. ChainMail: A Configurable Multimodal Lining to Enable Sensate Surfaces and Interactive Objects. In *Proceedings of the Fourth International Conference on Tangible, Embedded, and Embodied Interaction (TEI '10)*. 65–72. https://doi.org/10.1145/1709886.1709899

[55] Philipp Mittendorfer and Gordon Cheng. 2012. 3D surface reconstruction for robotic body parts with artificial skins. In *2012 IEEE/RSJ International Conference on Intelligent Robots and Systems*. 4505–4510. https://doi.org/10.1109/IROS.2012.6385559

[56] Cecilia Monoli, Juan Francisco Fuentez-Pérez, Nicola Cau, Paolo Capodaglio, Manuela Galli, and Jeffrey A. Tuhtan. 2021. Land and Underwater Gait Analysis Using Wearable IMU. *IEEE Sensors Journal* 21, 9, 11192–11202. https://doi.org/10.1109/JSEN.2021.3061623

[57] Elissa Morris, Daniel A McAdams, and Richard Malak. 2016. The state of the art of origami-inspired products: A review. In *International Design Engineering Technical Conferences and Computers and Information in Engineering Conference*, Vol. 50169. V05BT07A014.

[58] Niusha Navabian, Sherif Beskhyroun, and Justin Matulich. 2022. Development of wireless smart sensor network for vibration-based structural health monitoring of civil structures. *Structure and Infrastructure Engineering* 18, 3, 345–361. https://doi.org/10.1080/15732479.2020.1850801

[59] Andrei Nejur and Kyle Steinfeld. 2017. Ivy: Progress in developing practical applications for a weighted-mesh representation for use in generative architectural design. In *Proceedings of the 37th Annual Conference of the Association for Computer Aided Design in Architecture (ACADIA)*. 446– 455. http://papers.cumincad.org/cgi-bin/works/Show?acadia17_446

[60] Vinh P. Nguyen, Sang Ho Yoon, Ansh Verma, and Karthik Ramani. 2014. BendID: Flexible Interface for Localized Deformation Recognition. In *Proceedings of the 2014 ACM International Joint Conference on Pervasive and Ubiquitous Computing (UbiComp '14)*. 553–557. https://doi.org/10.1145/2632048.2636092

[61] Aditya Shekhar Nittala, Arshad Khan, Klaus Kruttwig, Tobias Kraus, and Jürgen Steimle. 2020. PhysioSkin: Rapid Fabrication of Skin-Conformal Physiological Interfaces. In *Proceedings of the 2020 CHI Conference on Human Factors in Computing Systems (CHI '20)*. 1–10. https://doi.org/10.1145/3313831.3376366

[62] Aditya Shekhar Nittala and Jürgen Steimle. 2022. Next Steps in Epidermal Computing: Opportunities and Challenges for Soft On-Skin Devices. In *Proceedings of the 2022 CHI Conference on Human Factors in Computing Systems (CHI '22)*. Article 389, 22 pages. https://doi.org/10.1145/3491102.3517668

[63] Jifei Ou, Daniel Oran, Don Derek Haddad, Joseph Paradiso, and Hiroshi Ishii. 2019. SensorKnit: Architecting Textile Sensors with Machine Knitting. *3D Printing and Additive Manufacturing* 6, 1, 1–11. https://doi.org/10.1089/3dp.2018.0122

[64] Davide Paloschi, Kirill A. Bronnikov, Sanzhar Korganbayev, Alexey A. Wolf, Alexander Dostovalov, and Paola Saccomandi. 2021. 3D Shape Sensing With Multicore Optical Fibers: Transformation Matrices Versus Frenet-Serret Equations for Real-Time Application. *IEEE Sensors Journal* 21, 4, 4599–4609. https://doi.org/10.1109/JSEN.2020.3032480

[65] Luis Paredes, Sai Swarup Reddy, Subramanian Chidambaram, Devashri Vagholkar, Yunbo Zhang, Bedrich Benes, and Karthik Ramani. 2021. FabHandWear: An End-to-End Pipeline from Design to Fabrication of Customized Functional Hand Wearables. *Proc. ACM Interact. Mob. Wearable Ubiquitous Technol.* 5, 2. https://doi.org/10.1145/3463518

[66] Brice Parilusyan, Marc Teyssier, Valentin Martinez-Missir, Clément Duhart, and Marcos Serrano. 2022. Sensurfaces: A Novel Approach for Embedded Touch Sensing on Everyday Surfaces. *Proc. ACM Interact. Mob. Wearable Ubiquitous Technol.* 6, 2. https://doi.org/10.1145/3534616

[67] Jung Jae Park, Phillip Won, and Seung Hwan Ko. 2019. A Review on Hierarchical Origami and Kirigami Structure for Engineering Applications. *International Journal of Precision Engineering and Manufacturing-Green Technology* 6, 1, 147–161. https://doi.org/10.1007/s40684-019-00027-2

[68] Narjes Pourjafarian, Marion Koelle, Bruno Fruchard, Sahar Mavali, Konstantin Klamka, Daniel Groeger, Paul Strohmeier, and Jürgen Steimle. 2021. BodyStylus: Freehand On-Body Design and Fabrication of Epidermal Interfaces. In *Proceedings of the 2021 CHI Conference on Human Factors in Computing Systems* (Yokohama, Japan) *(CHI '21)*. Article 504, 15 pages. https://doi.org/10.1145/3411764.3445475

[69] Narjes Pourjafarian, Marion Koelle, Fjolla Mjaku, Paul Strohmeier, and Jürgen Steimle. 2022. Print-A-Sketch: A Handheld Printer for Physical Sketching of Circuits and Sensors on Everyday Surfaces. In *Proceedings of the 2022 CHI Conference on Human Factors in Computing Systems* (New Orleans, LA, USA) *(CHI '22)*. Article 270, 17 pages. https://doi.org/10.1145/3491102.3502074

[70] Jing Qin, Li-Juan Yin, Ya-Nan Hao, Shao-Long Zhong, Dong-Li Zhang, Ke Bi, Yong-Xin Zhang, Yu Zhao, and Zhi-Min Dang. 2021. Flexible and Stretchable Capacitive Sensors with Different Microstructures. *Advanced Materials* 33, 34, 2008267. https://doi.org/10.1002/adma.202008267

[71] Sen Qiu, Hongkai Zhao, Nan Jiang, Donghui Wu, Guangcai Song, Hongyu Zhao, and Zhelong Wang. 2022. Sensor network oriented human motion capture via wearable intelligent system. *International Journal of Intelligent Systems* 37, 2, 1646–1673. https://doi.org/10.1002/int.22689

[72] Christian Rendl, David Kim, Sean Fanello, Patrick Parzer, Christoph Rhemann, Jonathan Taylor, Martin Zirkl, Gregor Scheipl, Thomas Rothländer, Michael Haller, and Shahram Izadi. 2014. FlexSense: A Transparent Self-Sensing Deformable Surface. In *Proceedings of the 27th Annual ACM Symposium on User Interface Software and Technology (UIST '14)*. 129–138. https://doi.org/10.1145/2642918.2647405

[73] Christian Rendl, David Kim, Patrick Parzer, Sean Fanello, Martin Zirkl, Gregor Scheipl, Michael Haller, and Shahram Izadi. 2016. FlexCase: Enhancing Mobile Interaction with a Flexible Sensing and Display Cover. In *Proceedings of the 2016 CHI Conference on Human Factors in Computing Systems (CHI '16)*. 5138–5150. https://doi.org/10.1145/2858036.2858314

[74] Bruce Richardson, Krispin Leydon, Mikael Fernstrom, and Joseph A. Paradiso. 2004. Z-Tiles: Building Blocks for Modular, Pressure-Sensing Floorspaces. In *CHI '04 Extended Abstracts on Human Factors in Computing Systems (CHI EA '04)*. 1529–1532. https://doi.org/10.1145/985921.986107

[75] Giovanni Saggio, Francesco Riillo, Laura Sbernini, and Lucia Rita Quitadamo. 2015. Resistive flex sensors: a survey. *Smart Materials and Structures* 25, 1, 013001. https://doi.org/10.1088/0964-1726/25/1/013001

[76] Philipp Schoessler, Sang-won Leigh, Krithika Jagannath, Patrick van Hoof, and Hiroshi Ishii. 2015. Cord UIs: Controlling Devices with Augmented Cables. In *Proceedings of the Ninth International Conference on Tangible, Embedded, and Embodied Interaction (TEI '15)*. 395–398. https://doi.org/10.1145/2677199.2680601

[77] Matthias Seuter, Alexandra Pollock, Gernot Bauer, and Christian Kray. 2020. Recognizing Running Movement Changes with Quaternions on a Sports Watch. *Proc. ACM Interact. Mob. Wearable Ubiquitous Technol.* 4, 4. https://doi.org/10.1145/3432197

[78] Fereshteh Shahmiri, Chaoyu Chen, Anandghan Waghmare, Dingtian Zhang, Shivan Mittal, Steven L. Zhang, Yi-Cheng Wang, Zhong Lin Wang, Thad E. Starner, and Gregory D. Abowd. 2019. Serpentine: A Self-Powered Reversibly Deformable Cord Sensor for Human Input. In *Proceedings of the 2019 CHI Conference on Human Factors in Computing Systems (CHI '19)*. 1–14. https://doi.org/10.1145/3290605.3300775

[79] Fereshteh Shahmiri and Paul H. Dietz. 2020. ShArc: A Geometric Technique for Multi-Bend/Shape Sensing. In *Proceedings of the 2020 CHI Conference on Human Factors in Computing Systems*. 1–12. https://doi.org/10.1145/3313831.3376269

[80] Shubham Sharma, Shubhankar Verma, Mohit Kumar, and Lavanya Sharma. 2019. Use of Motion Capture in 3D Animation: Motion Capture Systems, Challenges, and Recent Trends. In *2019 International Conference on Machine Learning, Big Data, Cloud and Parallel Computing (COMITCon)*. 289–294. https://doi.org/10.1109/COMITCon.2019.8862448

[81] Kwonsik Shin, Dongsu Kim, Hyunchul Park, Minkyung Sim, Hyunwoo Jang, Jung Inn Sohn, Seung Nam Cha, and Jae Eun Jang. 2020. Artificial Tactile Sensor With Pin-type Module for Depth Profile and Surface Topography Detection. *IEEE Transactions on Industrial Electronics* 67, 1, 637–646. https://doi.org/10.1109/TIE.2019.2912788

[82] Min Su, Pei Li, Xueqin Liu, Dapeng Wei, and Jun Yang. 2022. Textile-Based Flexible Capacitive Pressure Sensors: A Review. *Nanomaterials* 12, 9. https://doi.org/10.3390/nano12091495

[83] Haili Sun, Zhengwen Xu, Lianbi Yao, Ruofei Zhong, Liming Du, and Hangbin Wu. 2020. Tunnel Monitoring and Measuring System Using Mobile Laser Scanning: Design and Deployment. *Remote Sensing* 12, 4. https://doi.org/10.3390/rs12040730

[84] Lingyun Sun, Jiaji Li, Yu Chen, Yue Yang, Zhi Yu, Danli Luo, Jianzhe Gu, Lining Yao, Ye Tao, and Guanyun Wang. 2021. FlexTruss: A Computational Threading Method for Multi-Material, Multi-Form and Multi-Use Prototyping. In *Proceedings of the 2021 CHI Conference on Human Factors in Computing Systems* (Yokohama, Japan) *(CHI '21)*. Article 432, 12 pages. https://doi.org/10.1145/3411764.3445311

[85] Yu Sun, Yun Ye, Wu Liu, Wenpeng Gao, Yili Fu, and Tao Mei. 2019. Human Mesh Recovery From Monocular Images via a Skeleton-Disentangled Representation. In *Proceedings of the IEEE/CVF International Conference on Computer Vision (ICCV)*. 5349–5358.

[86] Shigeo Takahashi, Hsiang-Yun Wu, Seow Hui Saw, Chun-Cheng Lin, and Hsu-Chun Yen. 2011. Optimized Topological Surgery for Unfolding 3D Meshes. *Computer Graphics Forum* 30, 7, 2077–2086. https://doi.org/10.1111/j.1467-8659.2011.02053.x

[87] Ye Tao, Guanyun Wang, Caowei Zhang, Nannan Lu, Xiaolian Zhang, Cheng Yao, and Fangtian Ying. 2017. WeaveMesh: A Low-Fidelity and Low-Cost Prototyping Approach for 3D Models Created by Flexible Assembly. In *Proceedings of the 2017 CHI Conference on Human Factors in Computing Systems (CHI '17)*. 509–518. https://doi.org/10.1145/3025453.3025699

[88] Guanyun Wang, Fang Qin, Haolin Liu, Ye Tao, Yang Zhang, Yongjie Jessica Zhang, and Lining Yao. 2020. MorphingCircuit: An Integrated Design, Simulation, and Fabrication Workflow for Self-Morphing Electronics. *Proc. ACM Interact. Mob. Wearable Ubiquitous Technol.* 4, 4, 1–26. https://doi.org/10.1145/3432232

[89] Jiaxin Wang, Zhelong Wang, Fengshan Gao, Hongyu Zhao, Sen Qiu, and Jie Li. 2020. Swimming Stroke Phase Segmentation Based on Wearable Motion Capture Technique. *IEEE Transactions on Instrumentation and Measurement* 69, 10, 8526–8538. https:

//doi.org/10.1109/TIM.2020.2992183

[90] Irmandy Wicaksono, Elena Kodama, Artem Dementyev, and Joseph A. Paradiso. 2020. SensorNets: Towards Reconfigurable Multi-functional Fine-Grained Soft and Stretchable Electronic Skins. In *Extended Abstracts of the 2020 CHI Conference on Human Factors in Computing Systems (CHI EA '20)*. 1–8. https://doi.org/10.1145/3334480.3382866

[91] Grady Barrett Wright. 2003. *Radial basis function interpolation: Numerical and analytical developments*. Ph.D. University of Colorado at Boulder, Ann Arbor. https://www.proquest.com/dissertations-theses/radial-basis-function-interpolation-numerical/docview/305335254/se-2?accountid=15198

[92] Ruishu F. Wright, Mudabbir Badar, James C. Egbu, Ping Lu, Michael Buric, and Paul R. Ohodnicki Jr. 2019. Fully distributed optical fiber sensor for water and humidity monitoring. In *Fiber Optic Sensors and Applications XVI*, Vol. 11000. 1100007. https://doi.org/10.1117/12.2519239

[93] Zhonghua Xi, Yun-hyeong Kim, Young J. Kim, and Jyh-Ming Lien. 2016. Learning to segment and unfold polyhedral mesh from failures. *Computers & Graphics* 58, 139–149. https://doi.org/10.1016/j.cag.2016.05.022

[94] Fei Xu and Chengbo Mou. 2018. *Selected Topics on Optical Fiber Technologies and Applications*. BoD–Books on Demand.

[95] Zihan Yan, Jiayi Zhou, Yufei Wu, Guanhong Liu, Danli Luo, Zihong Zhou, Haipeng Mi, Lingyun Sun, Xiang 'Anthony' Chen, Ye Tao, Yang Zhang, and Guanyun Wang. 2022. Shoes++: A Smart Detachable Sole for Social Foot-to-Foot Interaction. *Proc. ACM Interact. Mob. Wearable Ubiquitous Technol.* 6, 2. https://doi.org/10.1145/3534620

[96] Pengtao Yu, Xin Li, Huayang Li, Youjun Fan, Jinwei Cao, Hailu Wang, Zihao Guo, Xuejiao Zhao, Zhonglin Wang, and Guang Zhu. 2021. All-Fabric Ultrathin Capacitive Sensor with High Pressure Sensitivity and Broad Detection Range for Electronic Skin. *ACS Applied Materials & Interfaces* 13, 20, 24062–24069. https://doi.org/10.1021/acsami.1c05478

[97] Tao Yu, Kaiwen Guo, Feng Xu, Yuan Dong, Zhaoqi Su, Jianhui Zhao, Jianguo Li, Qionghai Dai, and Yebin Liu. 2017. BodyFusion: Real-Time Capture of Human Motion and Surface Geometry Using a Single Depth Camera. In *Proceedings of the IEEE International Conference on Computer Vision (ICCV)*. 910–919.

[98] Hechuan Zhang, Zhiyong Chen, Shihui Guo, Juncong Lin, Yating Shi, Xiangyang Liu, and Yong Ma. 2020. Sensock: 3D Foot Reconstruction with Flexible Sensors. In *Proceedings of the 2020 CHI Conference on Human Factors in Computing Systems (CHI '20)*. 1–13. https://doi.org/10.1145/3313831.3376387

[99] Jinlu Zhang, Zhigang Tu, Jianyu Yang, Yujin Chen, and Junsong Yuan. 2022. MixSTE: Seq2seq Mixed Spatio-Temporal Encoder for 3D Human Pose Estimation in Video. In *Proceedings of the IEEE/CVF Conference on Computer Vision and Pattern Recognition (CVPR)*. 13232–13242.

[100] Qi Zhang, Yu Lu Wang, Yun Xia, Timothy Vernon Kirk, and Xiao Dong Chen. 2020. Textile-Only Capacitive Sensors with a Lockstitch Structure for Facile Integration in Any Areas of a Fabric. *ACS Sensors* 5, 6, 1535–1540. https://doi.org/10.1021/acssensors.0c00210

[101] Qi Zhang, Yu Lu Wang, Yun Xia, Peng Fei Zhang, Timothy V. Kirk, and Xiao Dong Chen. 2019. Textile-Only Capacitive Sensors for Facile Fabric Integration without Compromise of Wearability. *Advanced Materials Technologies* 4, 10, 1900485. https://doi.org/10.1002/admt.201900485

[102] Yuxiang Zhang, Liang An, Tao Yu, Xiu Li, Kun Li, and Yebin Liu. 2020. 4D Association Graph for Realtime Multi-Person Motion Capture Using Multiple Video Cameras. In *Proceedings of the IEEE/CVF Conference on Computer Vision and Pattern Recognition (CVPR)*. 1324–1333.

[103] Yuxiang Zhang, Zhe Li, Liang An, Mengcheng Li, Tao Yu, and Yebin Liu. 2021. Lightweight Multi-Person Total Motion Capture Using Sparse Multi-View Cameras. In *Proceedings of the IEEE/CVF International Conference on Computer Vision (ICCV)*. 5560–5569.

[104] Shufang Zhao, Wenhao Ran, Depeng Wang, Ruiyang Yin, Yongxu Yan, Kai Jiang, Zheng Lou, and Guozhen Shen. 2020. 3D Dielectric Layer Enabled Highly Sensitive Capacitive Pressure Sensors for Wearable Electronics. *ACS Applied Materials & Interfaces* 12, 28, 32023–32030. https://doi.org/10.1021/acsami.0c09893

[105] Junyi Zhu, Yunyi Zhu, Jiaming Cui, Leon Cheng, Jackson Snowden, Mark Chounlakone, Michael Wessely, and Stefanie Mueller. 2020. MorphSensor: A 3D Electronic Design Tool for Reforming Sensor Modules. In *Proceedings of the 33rd Annual ACM Symposium on User Interface Software and Technology (UIST '20)*. 541–553. https://doi.org/10.1145/3379337.3415898